J. Electrochem. Sci. Eng. **4(2)** (2014) 45-53; doi: **10.5599/jese.2014.0045**

Open Access : : ISSN 1847-9286

https://pub.iapchem.org/ojs/index.php/JESE

Original scientific paper

Synthesis and electrochemical performance of hierarchical Sb_2S_3 nanorod-bundles for lithium-ion batteries

XIAOZHONG ZHOU✉, SHUHUA HUA, LIANHUA BAI and DONG YU

Key Laboratory of Eco-Environment-Related Polymer Materials of Ministry of Education, Key Laboratory of Polymer Materials of Gansu Province, College of Chemistry and Chemical Engineering, Northwest Normal University, Lanzhou 730070, Gansu Province, P. R. China

✉Corresponding Author: E-mail: zxz20004@163.com; Tel.: +086 0931-7972663; Fax: +086 0931-7972663

Received: November 24, 2013; Revised: February 20, 2014; Published: May 13, 2014

Abstract

Uniform hierarchical Sb_2S_3 nanorod-bundles were synthesised successfully by L-cysteine hydrochloride-assisted solvothermal treatment, and were then characterised by X-ray diffraction, field emission scanning electron microscopy, and high-resolution transmission electron microscopy, respectively. The electrochemical performance of the synthesised Sb_2S_3 nanorod-bundles was investigated by cyclic voltammetry and galvanostatic charge–discharge technique, respectively. This material was found to exhibit a high initial charge specific capacity of 803 mA h g^{-1} at a rate of 100 mA g^{-1}, a good cyclability of 614 mA h g^{-1} at a rate of 100 mA g^{-1} after 30 cycles, and a good rate capability of 400 mA h g^{-1} at a rate of 500 mA g^{-1} when evaluated as an electrode candidate material for lithium-ion batteries.

Keywords

Sb_2S_3 nanorod-bundles, electrochemical performance, lithium-ion batteries

Introduction

Lithium-ion batteries (LIBs) are currently the most advanced rechargeable batteries for powering portable electronic devices such as laptop computers and cellular phones in view of their high energy density and benign design flexibility [1]. Nowadays, graphitic materials are extensively spread as commercial anode materials because of their low operating potential close to that of Li^+/Li and a good structural stability during cycling [2]. Unfortunately, the small theoretical specific capacity of the graphite anode ($Li_{1/6}C$, 372 mA h g^{-1}) restricts its future applications for powering electric vehicles (EVs). As a result, a lot of research efforts have been made to investigate various alternative anode materials with improved performance over the last decade [3]. Among alter-

native anode materials, metal sulfides have attracted particular attention because of their unique structures and high specific capacity [4,5].

As a typical metal sulfide, Sb_2S_3 is an important V-VI semiconductor. Owing to their prominent optical, photoelectronic and electrochemical properties, Sb_2S_3 nanomaterials can be potentially applied in photosensors [6], near-infrared optical devices [7], photoelectronic devices [8,9], lithium-ion batteries [10,11], etc. Zheng et al. synthesised Sb_2S_3 nanostructures with various dimensional nanostructures by a hydrothermal method and found that the reversible capacity of column-like superstructures, nanorods, and sheaf-like superstructures Sb_2S_3 electrodes are all around 700 mA h g^{-1} [10].

Recently, biomolecule-assisted synthetic routes have become a promising strategy in the preparation of various nanostructured materials because they are green chemistry approaches without toxic reagents and solvents and have obtained unique structures [12]. As an available biomolecule, L-cysteine has attracted considerable attention because of its special structure, which contains multifunctional groups ($–NH_2$, –SH, and –COO–) [13]. According to previous reports, L-cysteine can form a polymeric network structure under solution-phase reaction because its multifunctional groups can help to form interactions between L-cysteine molecules [14]. Besides, the presence of L-cysteine is critical to the formation of the final product, which showed excellent cycle stability with a high specific capacity and outstanding rate capability when used as a material for the anodes in lithium-ion batteries [15]. Therefore, it would be interesting to develop L-cysteine-assisted methods to prepare metal sulfide-based composites with excellent properties.

In this paper, we introduce a simple process for the fabrication of hierarchical Sb_2S_3 nanorod-bundles on the basis of a hydrothermal method assisted by L-cysteine hydrochloride (L-Cys·HCl). In this method, L-Cys·HCl can serve as a template, structure-directing agent and environmentally friendly sulfur source, while $SbCl_3$ serves as the antimony source. In addition, the formation mechanism of the Sb_2S_3 nanorod-bundles is also discussed, and it has been found that the hierarchical Sb_2S_3 nanorod-bundles exhibited high reversible capacity with good cyclic stability and high-rate capability.

Experimental

Synthesis

All chemicals were of analytical grade and were adopted without further purification. A typical solvothermal experiment for synthesising Sb_2S_3 material was conducted as follows. At first, 0.03 mol of L-cysteine hydrochloride with the formula $HSCH_2CH(NH_2)COOH·HCl$ and 0.01 mol of $SbCl_3$ were successively dissolved in 50 mL of anhydrous ethanol under magnetically stirring for 0.5 h in air. Next, the above-prepared solution was transferred to a 100 mL stainless steel Teflon-lined autoclave, followed by being sealed and then heated inside a conventional oven at 180 °C for 8 h. At last, after the autoclave was naturally cooled to room temperature, a black precipitate was collected by centrifugation and was then washed thoroughly successively with anhydrous ethanol and deionised water. The collected precipitate was dried in vacuum at 80 °C overnight for later uses.

Material characterisations

The structure, composition, and morphology of the as-prepared Sb_2S_3 material were characterised by powder X-ray diffraction (XRD, Rigaku D/max 2400, operating with Cu Kα radi-

ation of λ = 0.15416 nm), field emission scanning electron microscopy (FESEM, JEOL JSM-6701F, operating at 5 kV), and transmission electron microscopy (TEM, FEI TECNAI TF20, operating at 200 kV), respectively.

Electrochemical measurements

To evaluate the electrochemical performance of the as-prepared Sb_2S_3 material, galvanostatic charge-discharge (GSCD) and cyclic voltammetry (CV) techniques were employed. The GSCD technique was performed in the voltage range of 0.001-2.5 V *vs*. Li^+/Li on a battery testing system (LAND CT2001A, Wuhan Jinnuo Electronics Co., Ltd., China) at room temperatures. The CV technique was performed in the voltage range of 0.001-2.5 V *vs*. Li^+/Li at a scan rate of 0.2 $mV \cdot s^{-1}$ on an electrochemical workstation (Autolab PGSTAT128N, Metrohm, Switzerland) at room temperatures.

The testing electrodes were prepared by coating a copper foil substrate with a slurry comprising 80 wt. % active material of Sb_2S_3, 10 wt. % conducting additive of carbon black, and 10 wt. % binder of polyvinylidene fluoride (PVDF). This composition of the active material, the conducting additive, and the binder was found to be optimal for Sb_2S_3, The electrodes were cut into discs with a diameter of 10 mm, and then were assembled in a CR2032-type coin cell with a lithium foil as the counter electrode, a Celgard 2400 polypropylene foil as the separator, and a liquid solution of 1M $LiPF_6$ in ethylene carbonate (EC)/ethylmethyl carbonate (EMC)/dimethyl carbonate (DMC) (1:1:1 by volume, Shenzhen Capchem Technology Co., Ltd., China) as the electrolyte in an Ar-filled glove box. For clarification, discharging here refers to intercalation of Li into Sb_2S_3, whereas charging here refers to deintercalation of Li from Sb_2S_3.

Results and Discussion

Fig. 1 gives the XRD patterns of the as-prepared Sb_2S_3 and the standard peaks of Sb_2S_3 (JCPDS No. 42-1393). We can see that all of the obtained diffraction peaks could be well indexed to the orthorhombic Sb_2S_3 phase, and no obvious peaks of other crystalline phases were detected. This means that a well-crystallised form of Sb_2S_3 phase has been produced by our one-pot solvothermal treatment.

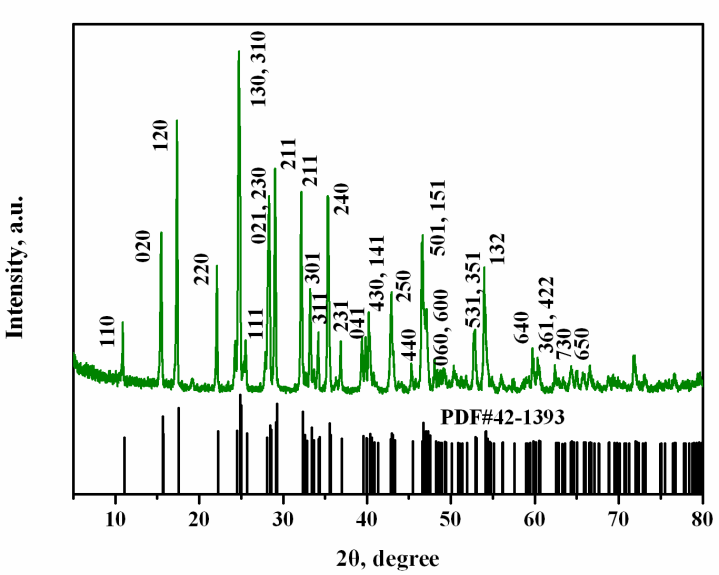

Figure 1. *XRD patterns of the as-prepared Sb_2S_3 material and standard peaks of Sb_2S_3 (JCPDS No. 42-1393)*

The morphology and structure of the as-prepared Sb_2S_3 material characterised by FESEM and TEM are presented in Fig. 2. It shows that the as-prepared Sb_2S_3 samples consist of cylindrical rods with a diameter of about 100 nm put into bundles. Fig. 2b shows the TEM and the relevant selected-area electron diffraction (SAED) patterns, which are composed of regular sharp diffraction spots characteristic of a single crystal of Sb_2S_3. This clearly implies that the nanorod grows preferentially along the [010] direction in a single crystalline form.

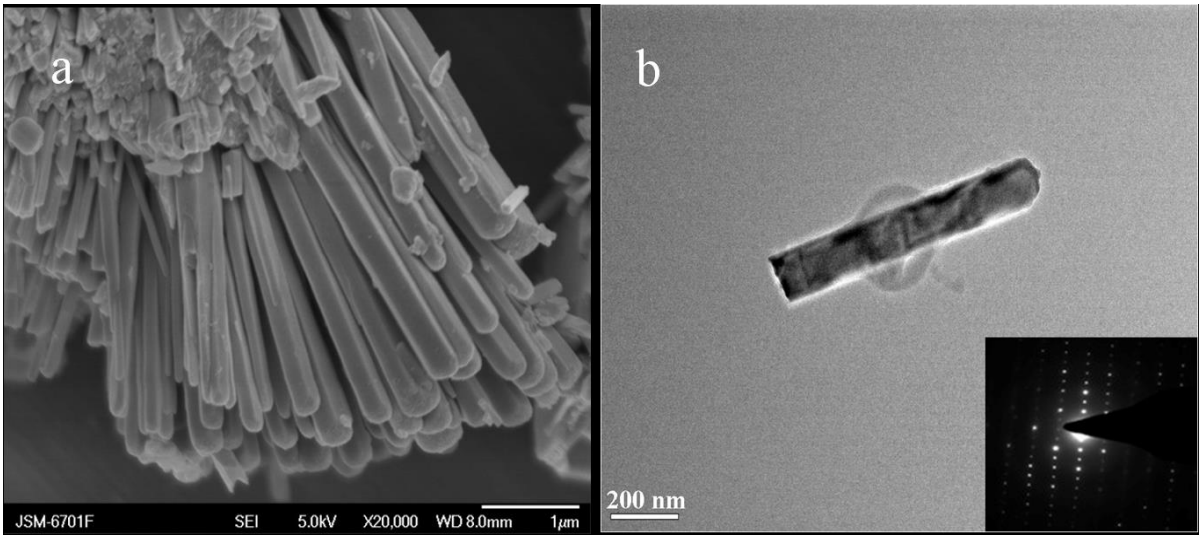

Figure 2. *Morphology and structure of the as-prepared Sb_2S_3 material characterised by* ***a*** *- FESEM and* ***b*** *- TEM*

Based on the previous results, it is reasonable to conclude that uniform hierarchical Sb_2S_3 nanorod-bundles are synthesised successfully by an L-Cys·HCl-assisted solvothermal treatment. L-Cys·HCl contains some multifunctional groups (-SH, $-NH_2$ and $-COO^-$) [16,17], which can be used for the conjugation of metallic ions or other functional groups [18]. When heated, L-Cys·HCl can release H_2S, which acts a sulfide source as well as a reducing agent, resulting in the formation of metal sulfide nanoparticles. The proposed growth process for the formation of hierarchical Sb_2S_3 nanorod-bundles is similar to the CoS nanowires [13], as shown in Fig. 3. And the reaction routes for the synthesis of Sb_2S_3 by L-Cys·HCl could be expressed as follows [12,19]:

$$HSCH_2CH(NH_2)COOH\cdot HCl + CH_3CH_2OH \rightarrow CH_3CH_2CH_2COCOOH + NH_4Cl + H_2S + H_2O \quad (1)$$

$$Sb^{3+} + H_2S + CH_3CH_2CH_2COCOOH \rightarrow Sb_2S_3 + SO_4^{2-} + CH_3COCOO^- + H_2O \quad (2)$$

The electrochemical properties of the as-prepared Sb_2S_3 material are first evaluated by a cyclic voltammetry (CV) test. Fig. 4 presents the CV curves of Sb_2S_3 sample for the initial three cycles in the voltage range of 2.5 to 0.001 V at a scanning rate of 0.2 mV s^{-1}. For the first cycle, there are two broad reduction peaks at around 1.0 and 0.4 V, respectively. The peak around 1.0 V can be attributed to the lithiation decomposition of the pristine Sb_2S_3 nanorods directly to fresh Sb and Li_2S. The peak around 0.4 V corresponds to the formation of Li_3Sb. Corresponding to the reduction peak, the oxidation peak at approximately 1.1 V was observed, which can be attributed to the dealloying process of Li_3Sb. Besides, three small and broad oxidation peaks at approximately 1.4 V, 1.9 V and 2.1 V may originate from the reconstruction of fresh Sb_2S_3 [10,11,20] and the transition of Li_2S into S, respectively, just as already found in CoSbS [21] and sulfide-graphene composite anodes [22].

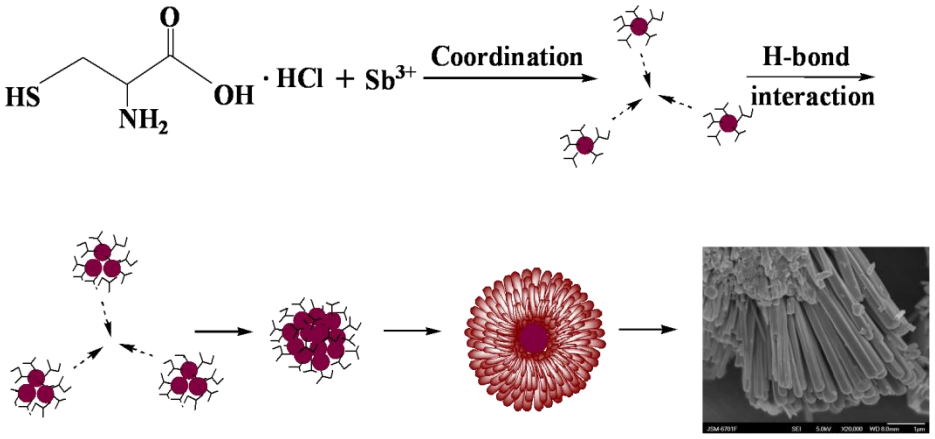

Figure 3. *The proposed growth process for formation of hierarchical Sb_2S_3 nanorod-bundles*

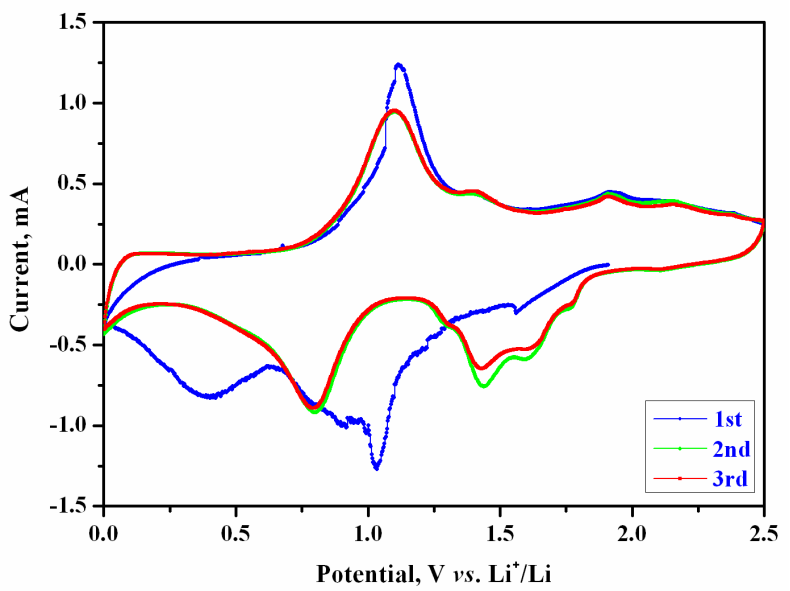

Figure 4. *CV curves of the as-prepared Sb2S3 material in the first three cycles at a scanning rate of 0.2 mV s−1*

From the second cycle on, we can see that the reduction peaks are different than that during the first cycle, which indicates a different electrochemical reduction mechanism. As shown in Fig. 4, the reduction and oxidation peaks at approximately 0.8 and 1.1 V originate from the alloying and dealloying process of fresh Sb metallic particles, respectively. The others are attributed to the decomposition/reconstruction of fresh Sb_2S_3 [10,11,20] and the electrochemical conversion between S and Li_2S [21,22]. Apparently, all the reduction peaks have their corresponding counterparts of oxidation peaks; this result suggests that the nanosized fresh Sb_2S_3 phase could be reversibly reconstructed and re-decomposed during repeated charging and discharging processes.

The potential profiles of the as-prepared Sb_2S_3 sample in cycles 1, 2, 5, 10, 30 and 49 are shown in Fig. 5. We can see that the discharging potential plateaus in the first cycle differ evidently from the following cycles, implying a different lithiation mechanism in the first cycle. This is in good agreement with the above CV analysis. The first discharging and charging specific capacities are 1166 mA h g^{-1} and 803 mA h g^{-1}, respectively, and the initial capacity loss could come from the irreversible loss of lithium ions due to the formation of a solid electrolyte interphase (SEI) layer [23], and the partial irreversibility of the electrochemical reaction (3) [20]. The initial coulombic efficiency is 68.9 %, which is higher than that (50 %) of alloying-dealloying mechanism.

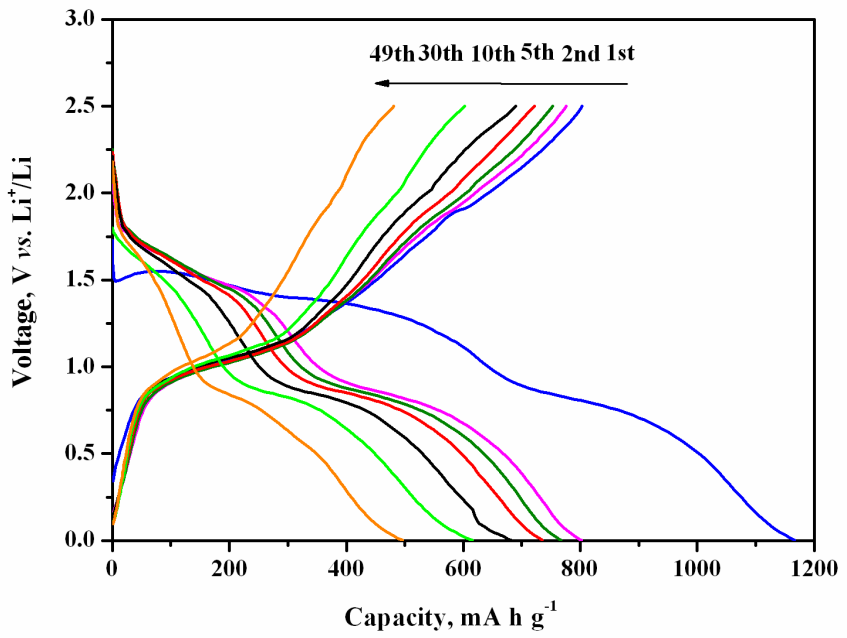

Figure 5. *Potential profiles of the as-prepared Sb_2S_3 sample in cycles 1, 2, 5, 10, 30 and 49 at a current density of 100 mA g^{-1}*

The cycle performance of the as-prepared Sb_2S_3 material at a current density of 100 mA g^{-1} is shown in Fig. 6. We can see that the Sb_2S_3 material displays a reversible capacity of 614 mA h g^{-1} even in the 30th cycle, the capacity retention after the 30th cycle is approximately 74.9 % with respect to the first charging specific capacity. During the cycling, the discharging specific capacity is slightly larger than the previous charging specific capacity, indicating that the electrode material becomes gradually activated, and this is beneficial to the capacity retention. These excellent electrochemical characteristics might be attributed to its special structure and smaller size of the nanorods. The sheaf-like Sb_2S_3 superstructures are composed of nanorods with a relatively smaller diameter; this special structure favors both the diffusion of the lithium ion and the electrolyte and Sb_2S_3.

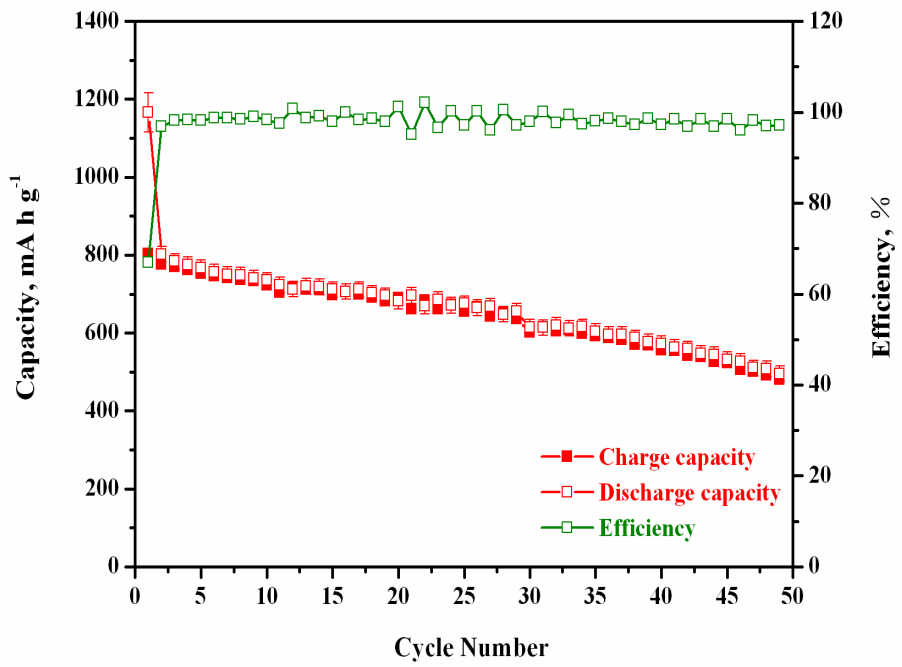

Fig. 6. *Cycle performance of the as-prepared Sb_2S_3 material at a current density of 100 mA·g^{-1}.*

The entire reaction in relation to Sb_2S_3 can be expressed as the following reaction [10,11,20-22].

$$Sb_2S_3 + 6Li^+ \leftrightarrow 2Sb + 3Li_2S \quad (3)$$

$$2Sb + 6Li^+ \leftrightarrow 2Li_3Sb \quad (4)$$

$$Li_2S \leftrightarrow Li^+ + S \quad (5)$$

The reversible specific capacity of the Sb_2S_3 is 473 mA h g^{-1} if we only consider the reversible reaction (3). However, if we consider both the reversible reactions (3) and (4), the reversible specific capacity of the Sb_2S_3 can be achieved as high as 946 mA h g^{-1}. In our work, the first reversible specific capacity of the Sb_2S_3 sample is as high as 803 mA h g^{-1}, and 68.9 % can be achieved for the initial coulombic efficiency. This suggests that our as-prepared Sb_2S_3 undergoes both the conversion reaction mechanism and alloying-dealloying lithiation mechanism, which contributes to the nanometer-sized effect. According to the nanometer-sized effect, the nanosized electrode material could have reactive activity. As a result, the reduction and oxidation of metal antimony could be observed, and the electrode exhibited larger capacity and better cycling performance than powder electrode [24].

The rate capability of the as-prepared Sb_2S_3 material is reflected in Fig. 7. We can see that the Sb_2S_3 material displays a good rate capability of 400 mA h g^{-1} at a current density of 500 mA g^{-1}. But when the charge/discharge current density changes from 1000 to 50 mA g^{-1}, the specific capacities of the Sb_2S_3 materials cannot return to the last values; the major reason for capacity fading is that Li_2S formed during the first discharge reaction and Li_2S_x (x>1, lithium polysulfide) are known to dissolve in the electrolyte [25]. A promising route to circumvent this drawback is by producing composite carbon materials whereby the carbon network provides good conductivity, prevents Li_2S and Li_2S_x from dissolving in the electrolyte and buffers the large volume changes induced by charging [26-28].

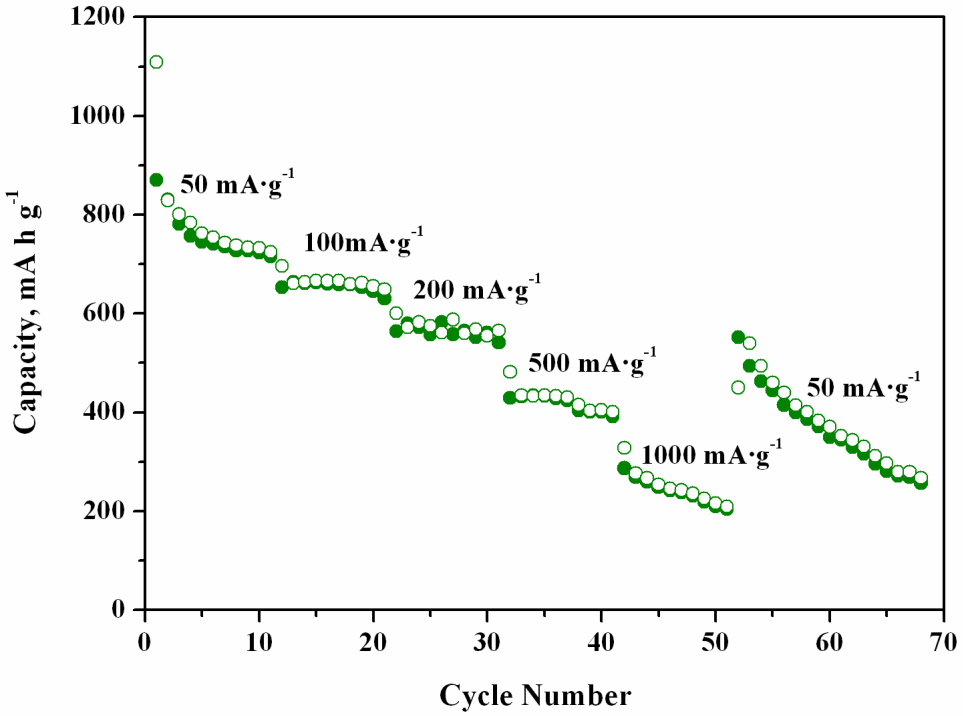

Fig. 7. *Potential profiles of the as-prepared Sb_2S_3 material at varying current densities*

Conclusions

In summary, uniform hierarchical Sb_2S_3 nanorod-bundles are synthesised successfully by a L-cysteine hydrochloride-assisted solvothermal treatment. The presence of L-cysteine is critical to the formation of the Sb_2S_3 material, which is found to display a high lithiation and delithiation specific capacity of 1166 and 803 mA h g^{-1} at a current density of 100 mA g^{-1}, a good cyclability of 614 mA h g^{-1} at a current density of 100 mA g^{-1} after 30 cycles, and a superior rate capability of 400 mA h g^{-1} at a current density of 500 mA g^{-1} when evaluated as an electrode candidate material for lithium-ion batteries. This good lithium storage performance can be ascribed to the nanosized structure. In addition, the preparative method could be a universal green chemistry approach to the synthesis of other metal sulfides.

***Acknowledgements**: Financial supports from the specialized research fund for the doctoral program of higher education of China under grant No. 20116203120005 and the natural science foundation of Gansu Province under grant No. 1107RJZA147 are acknowledged.*

References

[1] J. M. Tarascon and M. Armand, *Nature* **414** (2001) 359-367.
[2] M. Noel and V. Suryanarayanan, *J. Power Sources* **111** (2002) 193-209.
[3] W.-J. Zhang, *J. Power Sources* **196** (2011) 13-24.
[4] H. Hwang, H. Kim and J. Cho, *Nano Letters* **11** (2011) 4826-4830.
[5] J. Xiao, D. Choi, L. Cosimbescu, P. Koech, J. Liu and J. P. Lemmon, *Chem. Mater.* **22** (2010) 4522-4524.
[6] X. B. Cao, L. Gu, W. C. Wang, W. J. Gao, L. J. Zhuge and Y. H. Li, *J. Cryst. Growth* **286** (2006) 96-101.
[7] G. Y. Chen, W. X. Zhang and A. W. Xu, *Mater. Chem. Phys.* **123** (2010) 236-240.
[8] W. J. Lou, M. Chen, X. B. Wang and W. M. Liu, *Chem. Mater.* **19** (2007) 872-878.
[9] G. Y. Chen, B. Dneg, G. B. Cai, T. K. Zhang, W. F. Dong, W. X. Zhang and A. W. Xu, *J. Phys. Chem. C* **112** (2008) 672-679.
[10] J. M. Ma, X. C. Duan, J. B. Lian, T. Kim, P. Peng, X. D. Liu, Z. F. Liu, H. B. Li and W. J. Zheng, *Chem. Eur. J.* **16** (2010) 13210-13217.
[11] C. M. Park, Y. Hwa, N. E. Sung and H. J. Sohn, *J. Mater. Chem.* **20** (2010) 1097-1102.
[12] K. Chang and W. X. Chen, *ACS Nano* **5** (2011) 4720-4728.
[13] S.-J. Bao, C. M. Li, C.-X. Guo and Y. Qiao, *J. Power Sources* **180** (2008) 676-681.
[14] X. Y. Chen, H. L. Li, S. M. Wang, M. Yang and Y. X. Qi, *Mater. Lett.* **66** (2012) 22-24.
[15] S.-K. Park, S.-H. Yu, S. Woo, J. Ha, J. Shin, Y.-E. Sung and Y. Z. Piao, *Cryst.Eng. Comm* **14** (2012) 8323-8325.
[16] B. Zhang, X. Ye, W. Hou, Y. Zhao and Y. Xie, *J. Phys. Chem. B* **110** (2006) 8978-8985.
[17] S. Xiong, B. Xi, D. Xu, C. Wang, X. Feng, H. Zhou and Y. Qian, *J. Phys. Chem. C* **111** (2007) 16761-16767.
[18] J. Jiang, R. Yu, R. Yi, W. Qin, G. Qiu and X. Liu *J Alloy Compd* **493** (2010) 529-534.
[19] X.-L. Li and Y.-D. Li, *J. Phys. Chem. B* **108** (2004) 13893-13900.
[20] H. Yang, X. Su and A. Tang, *Mater. Res. Bull.* **42** (2007) 1357-1363.
[21] J.-O. Lee, J.-U. Seo, J.-H. Song, C.-M. Park and C.-K. Lee, *Electrochem. Commun.* **28** (2013) 71-74.
[22] M. Zhang, D. Lei, X. Z. Yu, L. B. Chen, O. H. Li, Y. G. Wang, T. H. Wang and G. Z Cao, *J. Mater. Chem.* **22** (2012) 23091-23097.
[23] J. Yan, B. J. Xia, Y. C. Su, X. Z. Zhou, J. Zhang and X. G. Zhang, *Electrochim. Acta* **53** (2008) 7069-7078.

[24] M.-Z. Xue and Z.-W. Fu, *Electrochem. Commun.* **8** (2006) 1250-1256.
[25] J.-S. Chung, H.-J. Sohn, *J. Power Sources* **108** (2002) 226-231.
[26] P. V. Prikhodchenko, J. Gun, S. Sladkevich, A. A. Mikhaylov, O. Lev, Y. Y. Tay, S. K. Batabya and D. Y. W. Yu, *Chem. Mater.* **24** (2012) 4750-4757.
[27] K. Chang, Z. Wang, G. Huang, H. Li, W. Chen and J. Y. Lee, *J. Power Sources* **201** (2012) 259-266.
[28] K.-J. Huang, L. Wang, J. Li and Y.-M. Liu, *Sens. Actuators, B* **178** (2013) 671-677.